Proceedings of the Indian National Science Academy (2026) 92:1329–1337
https://doi.org/10.1007/s43538-025-00490-3

RESEARCH PAPER

Aspect ratio-dependent anti-bacterial and anti-biofilm potential of plasmonic gold nanostructures

Harshita Agarwal[1] · Rishabh Kumar Srivastava[1] · Raviraj Vankayala[1,2] · Neha Jain[1]

Received: 27 January 2025 / Accepted: 24 June 2025 / Published online: 15 July 2025
© Indian National Science Academy 2025

Abstract
Antibiotic resistance poses a major global health threat, with biofilm formation being a critical factor. Biofilms are microbial communities where the cells are protected from adverse environmental conditions and provide a fitness advantage over the free-living planktonic cells via encapsulation in extra polymeric substance (EPS). EPS provides resistance to antimicrobials by providing a physical barrier, horizontal gene transfer, and altering microbial behavior, limiting the treatment regime for biofilms and suggesting a dire need for alternative therapeutic interventions. In the present study, we harnessed the efficacy of plasmonic gold nanostructures such as nanoparticles (AuNPs) and nanorods (AuNRs) to prevent bacterial growth and biofilm formation. Our study elucidates that high aspect ratio nanorods, AuNR(H), display better anti-bacterial activity as compared to low aspect ratio nanorods, AuNR(L), and AuNPs against *Escherichia coli*, *Pseudomonas aeruginosa*, *Bacillus subtilis*, and *Staphylococcus aureus*. We further investigated the efficacy of AuNR(H) in inhibiting bacterial growth by photothermal and photodynamic mechanisms. The prevention of the formation of resilient biofilms by AuNR(H) was characterized by crystal-violet staining and microscopy. Our findings demonstrate that the anti-bacterial and anti-biofilm activities of plasmonic gold nanostructures depend on their morphologies and aspect ratio, as a higher aspect ratio may offer an increased surface area for bacterial attachment and contact killing. We believe that results will pave the way for the potential use of plasmonic nanostructures with current therapeutics to reduce the burden of biofilm-related infections.

Keywords Anti-microbial resistance · Bacterial growth · Biofilm · Gold-nanostructures

Introduction

Bacterial growth is a complex cycle of cellular replication, transitioning through lag, exponential, stationary, and death phases, modulated by environmental conditions such as nutrient availability and stress factors (Rolfe et al. 2012). However, when environmental conditions become challenging, bacteria employ a survival strategy and form biofilm (Agarwal et al. 2025). Biofilms are intricate, multicellular aggregates encased in an extracellular polymeric substance (EPS) matrix, adhering to biotic and abiotic surfaces. While biofilms represent a successful bacterial adaptation, they also pose significant challenges, particularly in healthcare and industrial settings (Agarwal et al. 2025).

Bacteria in a planktonic state are relatively vulnerable to antibiotics and environmental changes. However, the transition to a biofilm state significantly alters their behavior (Sharma et al. 2023). Biofilm formation begins with the attachment of bacterial cells to a substrate, followed by EPS secretion and the development of a three-dimensional structure (Sharma et al. 2023). Biofilms are directly linked to persistent infections caused by *Staphylococcus aureus*, *Pseudomonas aeruginosa*, *Klebsiella pneumoniae*, and *Escherichia coli*. Their presence on medical devices, such as catheters and implants, further complicates treatments, often requiring surgical intervention and increasing healthcare costs (Mishra et al. 2024).

✉ Neha Jain
njain@iitj.ac.in

[1] Department of Bioscience and Bioengineering, Indian Institute of Technology Jodhpur, Karwar, Rajasthan 342030, India

[2] Interdisciplinary Research Division Smart Healthcare, Indian Institute of Technology Jodhpur, Karwar, Rajasthan 342030, India

Biofilms significantly contribute to antibiotic resistance through a combination of physical, chemical, and biological mechanisms that protect the embedded bacterial communities (Liu et al. 2024). Their EPS matrix, a complex blend of polysaccharides, proteins, and nucleic acids, serves as a physical barrier to antibiotics, hindering their penetration into the biofilm interior. This limited diffusion allows only sub-lethal concentrations of antibiotics to reach the deeper layers, fostering a selective environment that promotes the survival and proliferation of resistant strains (Agarwal et al. 2025; Azeem et al. 2025).

The persistence of biofilm-associated infections, such as those on medical devices or chronic wounds, underscores the need for innovative therapeutic strategies, and biofilm-specific inhibitors, to overcome these formidable defences (Sahoo and Meshram 2024). The development of biofilm-resistant strategies has seen a surge in interest in nanotechnology, particularly plasmonic nanoparticles. Among various plasmonic nanostructures, gold nanostructures have demonstrated exceptional potential due to their unique optical properties, biocompatibility, and ability to disrupt bacterial growth and biofilm structures and act through multiple mechanisms, including disrupting bacterial membranes, generating reactive oxygen species (ROS), and inhibiting quorum sensing (Saed et al. 2024). Our study explores the role of plasmonic nanoparticles, particularly through the lens of spatial configuration and efficacy, in preventing bacterial growth and biofilm formation. Our investigation demonstrates the comparative analysis of different aspect ratios of nanorods to that of the nanoparticles against different resistant bacteria and implies that high aspect ratio nanorods are more effective than low aspect ratio nanorods and nanoparticles at similar concentrations. We further analyzed the efficacy of high aspect ratio gold nanorods through different mechanisms like photothermal and photodynamic effects. We also investigated the role of high aspect ratio nanorods against biofilm formation. Our results on exploration of plasmonic gold nanoparticle configurations hold promise for tailoring strategies against pathogenic bacteria and biofilms.

Methodology

Synthesis of AuNRs and AuNPs

Gold nanorods (AuNRs) were prepared using the well-established seed-mediated methodology (Johnson et al. 2002). This method allows the aspect ratio of gold nanorods to be tuned, resulting in well-dispersed nanorods. First, a surfactant, cetyltrimethylammonium bromide (CTAB), was used to cap the prepared gold seeds. CTAB is used as a shape-directing agent and is essential for the anisotropic growth of AuNRs in seed-mediated synthesis. The concentration of CTAB (along with other reagents like silver nitrate and ascorbic acid) directly influences the aspect ratio (length-to-width ratio) of the nanorods, which is a critical factor in determining the longitudinal surface plasmon resonance (LSPR) wavelength. Concentration of CTAB was 0.2 M, and it was mixed with a solution of 0.5 mM $HAuCl_4 \cdot 3H_2O$. The entire reaction was kept under constant stirring at ambient conditions, and 30 µL of ice-cold sodium borohydride (0.01 M concentration) was added. Eventually, the prepared sample turned yellow-brown or dark yellow in color, indicating that the gold seeds were successfully formed. Following this, the growth phase began with the addition of 5 mL of 0.2 M [RA1] along with 5 mL of 1 mM $HAuCl_4 \cdot 3H_2O$, and different volumes of 4 mM $AgNO_3$ were used (AR 3.1 and AR 3.7). During the reaction, 0.0788 M ascorbic acid was added while keeping the sample under gentle stirring. Both sodium borohydride and ascorbic acid act as reducing agents at different stages of gold nanorod formation. Finally, 120 µL of gold seeds were added, with the seed size typically up to or less than 10 nm. Once the reaction was complete, the gold nanorods were collected and pelleted using a centrifuge at 10,000 rpm for 10 min (REMI RM-03 PLUS). This step was performed to remove the toxic CTAB, although a small amount of CTAB remains to prevent the aggregation of the gold nanorods. The quantity of $AgNO_3$ can be varied to tune the aspect ratio.

To prepare gold nanoparticles (AuNPs), a 0.2 M $HAuCl_4 \cdot 3H_2O$ solution was mixed in deionized (DI) water to make a total volume of about 20 mL. The mixture was heated with constant moderate stirring. Once the temperature reaches high and the entire solution starts to boil, 1% w/v trisodium citrate (TSC) is added drop by drop. On TSC addition, the solution gradually turned purplish black. The reaction continued for some time until the solution turned wine red, indicating the reaction was complete. The solution was then centrifuged at 15,000 rpm (REMI RM-03 PLUS) for 10 min. The washing step was repeated 1–2 times, and the isolated nanoparticles were resuspended in DI water. The concentration of gold nanorods (AuNRs) and gold nanoparticles (AuNPs) was calculated using pre-established calculation methods (Liu et al. 2007). We have made sure that the concentration of AuNRs and AuNPs for a given volume of the sample is the same. The detailed calculations for the concentrations are given in supplementary information (SI 1).

Growth conditions and growth curves for bacterial species

Bacillus subtilis, Methicillin-resistant *S. aureus* (MRSA), *E. coli* UT189, and *P. aeruginosa* were used as representative microorganisms for Gram +ve and Gram −ve strains, respectively. Cultures were prepared from glycerol stock by four-way streaking on Luria broth (LB) agar plate. After overnight incubation, a single colony was used to inoculate the sterile LB. The inoculating broths were then incubated at 37 °C and 200 rpm till O.D. 600 nm reached 1. The antimicrobial effect of the plasmonic gold nanorods with and without laser irradiation was determined. Primary cultures of bacterial species were diluted till O.D. 600 nm reached 0.05 in LB media in the 96 well plates. Bacterial cultures at OD 0.05 were treated with plasmonic gold nanoparticles at various concentrations in dark and light irradiation. The 808 nm laser power density used for irradiation was 1 W/cm^2. All experiments were conducted in triplicates.

Reactive oxygen species (ROS) generation

ROS produced in the *E. coli* and *B. subtilis* bacterial cells was estimated using 2′,7′-dichlorofluorescein diacetate (DCFH-DA). The ROS generation due to plasmonic gold nanorods with and without laser irradiation was determined. The bacterial cell suspension was treated with AuNR(H) alone and light-activated AuNR(H) and incubated at 37 °C for 4 h along with the control. For light activation, an 808 nm laser with a power of 1 W/cm^2 was used. After 4 h of incubation, bacterial cells were centrifuged at 7300 g for 10 min, followed by the treatment of supernatant with 50 mM of DCFH-DA and kept at 37 °C for 1 h in dark condition. The formation of ROS due to AuNR(H) was detected using the fluorescence microtiter plate reader (SpectraMax M2^e) with excitation and emission wavelengths of 490 and 520 nm, respectively.

Biofilm preparation

For the preparation of *B. subtilis* and *E. coli* biofilms, four-way streaking was performed from glycerol stocks in LB, and the plates were incubated for 8 to 12 h at 37 °C. Isolated colonies from the plate were inoculated in 2 ml of LB media, and the primary culture was incubated at 37 °C for 12 to 14 h with shaking at 200 rpm. For *B. subtilis* biofilm, after 14 h, 1 ml of LBGM media (LB supplemented with 1% of glycerol (v/v); 100 µM $MnSO_4$), and 2 µl of primary culture were added in 96 well plates, parafilm and stirred gently on the rocker for 3 min. The culture was then incubated at 30 °C for 48 h, and the floating pellicle biofilms at the media-air interface were observed. For *E. coli* biofilms, after 14 h, 1 ml YESCA (yeast extract-Casamino Acids) media + 4% DMSO and 2 µl of primary culture were added in 96 well plates, parafilm and stirred gently on the rocker for 3 min. The culture was then incubated at 26 °C for 5 days, and the floating pellicle biofilms on the media-air interface were observed. Biofilms formed by both the microorganisms were also inspected for the effect of AuNR(H); under similar conditions, in the presence of various concentrations of AuNR(H), biofilms formed with the addition of MilliQ are taken as control. For staining of biofilms, the media was gently removed, and 800 µl of a 0.1% solution of crystal violet (CV) prepared in water was added to each well of the microtiter plate containing biofilms. Following the addition of the dye, the microtiter plate was incubated at room temperature for 10–15 min and then thoroughly rinsed with water 3–4 times. The biofilms were dried overnight. For the quantification of biofilms, 200 µl of 33% glacial acetic acid in water was added to each well to solubilize the CV. The microtiter plate was then incubated at room temperature for 10–15 min. On completion of the period of incubation,10 µl of the solubilized CV with 90 µl glacial acetic acid was transferred to a new flat-bottomed microtiter plate, and absorbance was recorded in a plate reader at 595 nm using 33% acetic acid in water as the blank.

Field emission scanning electron microscopy (FE-SEM) characterization

To characterize the morphology, biofilms of *E. coli* and *B. subtilis* without and with AuNR(H) were fixed in 2% glutaraldehyde solution overnight at 4 °C and then rinsed in 1X PBS. All the samples were dehydrated at 5-minute intervals in a graded series (30–90%) and finally in 100% ethanol. After dehydration samples were placed on silicon wafers and dried for 1 h at room temperature in the desiccator. Samples on wafers were mounted onto carbon sticky tape on top of aluminum stubs and sputter-coated with silver and imaged using an Everhart–Thornley detector (ETD) in a field-emission scanning electron microscope (Apreo 2 S from Thermo Fisher Scientific) at an accelerating voltage of 10 kV and 15 kV and 8000× magnification.

Data plotting and statistical analysis

The data were plotted, normalized, and analyzed using Origin Pro V9 software. All the statistical *p*-values were calculated using a two-tailed *t*-test.

Results

Physicochemical characterization of AuNPs and AuNRs

Using a JASCO V-770 spectrophotometer, the gold nanorods (AuNRs) were analyzed using UV-Vis absorption spectroscopy. In the UV-Vis absorption spectrum of AuNRs, there were two peaks related to surface plasmon resonance (SPR): one peak was along the length of the nanorods (longitudinal SPR, LSPR) and the other along their width (transverse SPR, TSPR). The LSPR wavelength of the AuNRs can be red-shifted as the aspect ratio increases. In Fig. 1A, the AuNRs with an aspect ratio (AR) of 3.1 showed a transverse surface plasmon resonance (TSPR) peak at 522 nm and a longitudinal surface plasmon resonance (LSPR) peak at 774 nm. Similarly, the AuNRs with an AR of 3.7 had a TSPR peak at 526 nm and an LSPR peak at 822 nm, which indicated a noticeable shift in the LSPR peak (Murphy et al. 2005). Additionally, images of these AuNRs with different aspect ratios were captured using Field-emission Scanning Electron Microscopy (FE-SEM) (Fig. 1B, C). We have analyzed multiple SEM images using ImageJ to determine the average length and diameter of the AuNR(H) and AuNR(L). Using UV-Vis and FE-SEM, the spherical gold nanoparticles were also characterized (Fig. 1A, D). The plasmonic peak for the spherical gold nanoparticle is centered at 528 nm.

Effect of AuNPs and different aspect ratio AuNRs on bacterial growth

Next, we studied the anti-bacterial activity of synthesized AuNPs and AuNRs by analyzing their effects on the growth kinetics of bacteria. For the present study, we selected uropathogenic *Escherichia coli* (*E. coli* UTI89), *Pseudomonas aeruginosa* (*P. aeruginosa*), methicillin-resistant *Staphylococcus aureus* (MRSA), and *Bacillus subtilis* (*B. subtilis*) due to their clinical and environmental relevance. *E. coli* UTI89 is a representative Gram-negative bacterium commonly found in urine and bladder infections. *P. aeruginosa*, another Gram-negative pathogen, is known for its antibiotic resistance and association with deadly infections. MRSA serves as a model bacterium for Gram-positive

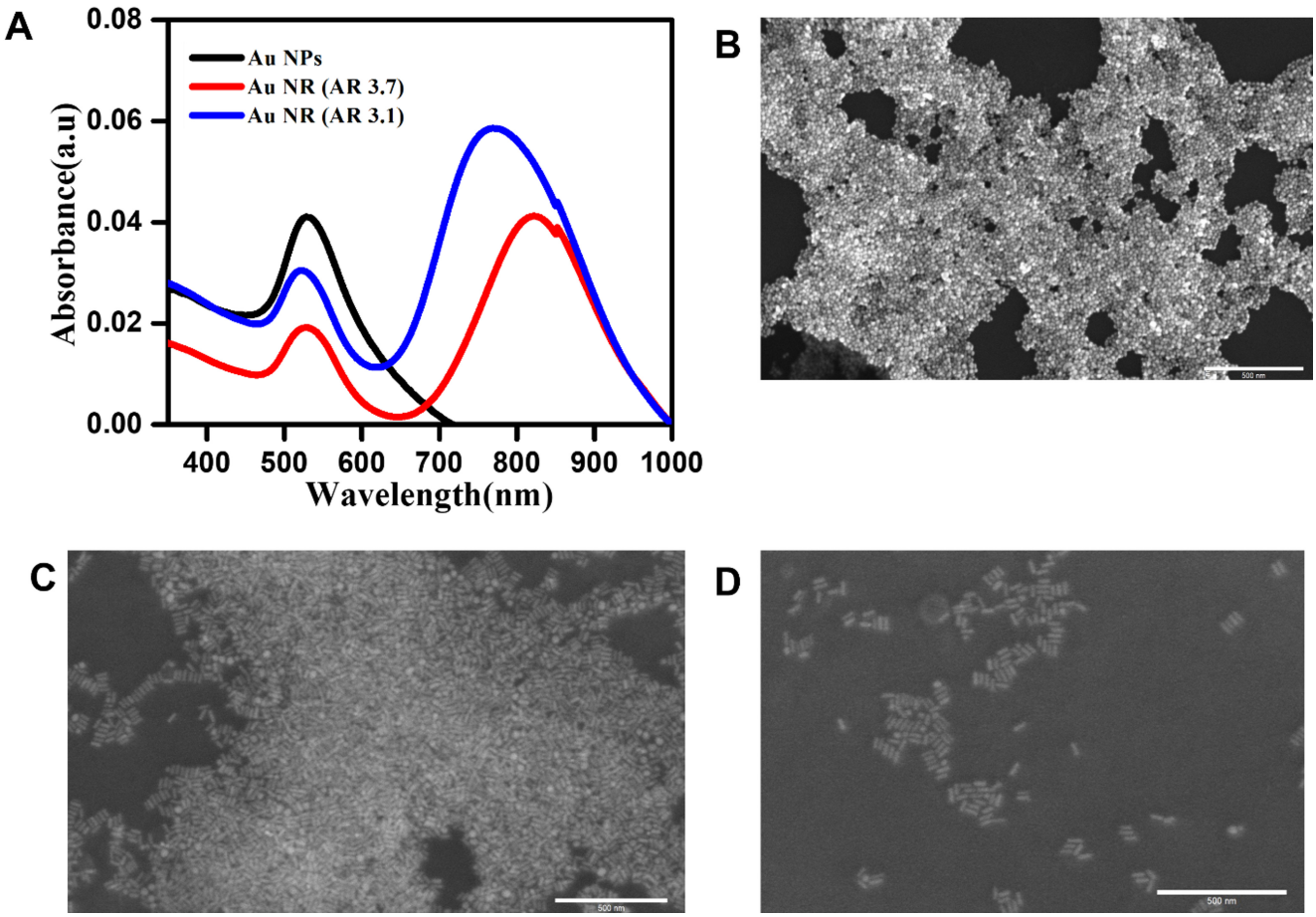


Fig. 1 Physicochemical characterization of AuNPs and AuNRs with various LSPR peaks. **A** UV–vis-NIR absorption spectra. **B**–**D** FE-SEM images of plasmonic AuNPs and AuNRs with three different aspect ratios (3.1 and 3.7). Scale bar = 500 nm

multidrug-resistant pathogens, highlighting the need for innovative anti-bacterial agents. *B. subtilis*, a non-pathogenic Gram-positive bacterium, is included in studies for comparative analysis of Gram-positive bacterial susceptibility. These organisms provided a comprehensive assessment of the anti-bacterial spectrum of gold nanostructures against both Gram-positive and Gram-negative bacteria, elucidating their potential in diverse applications. The growth inhibition of bacterial species was evaluated across a range of AuNP and AuNRs concentrations to determine their concentration-dependent anti-bacterial efficacy. As shown in Fig. 2A Panel 1, AuNR(H) at a concentration of 1 nM completely inhibited *E. coli* growth; however, lower concentrations were not effective. Other nanostructures such as AuNR(L) and AuNPs did not show any inhibitory effect at any concentrations (Fig. 2A Panels 2 and 3). AuNR(H) were effective against *P. aeruginosa* growth at a higher concentration. At 2 nM concentration of AuNR(H), the lag phase of *P. aeruginosa* growth increased from 1 to 2 h to 3–4 h and at 5 nM concentration of AuNR(H) there was complete inhibition of *P. aeruginosa* growth as shown in Fig. 2B Panel 1. Similar higher concentrations of AuNR(L) and AuNPs were not able to influence the growth of *P. aeruginosa* (Fig. 2B Panels 2 and 3). Next, we checked the efficacy of nanostructures in inhibiting the growth of Gram-positive bacteria. With *B. subtilis*, a lower concentration of AuNR(H) (0.2 nM) increased the lag phase from 1 h to 4 h, whereas a higher concentration (0.6 nM)

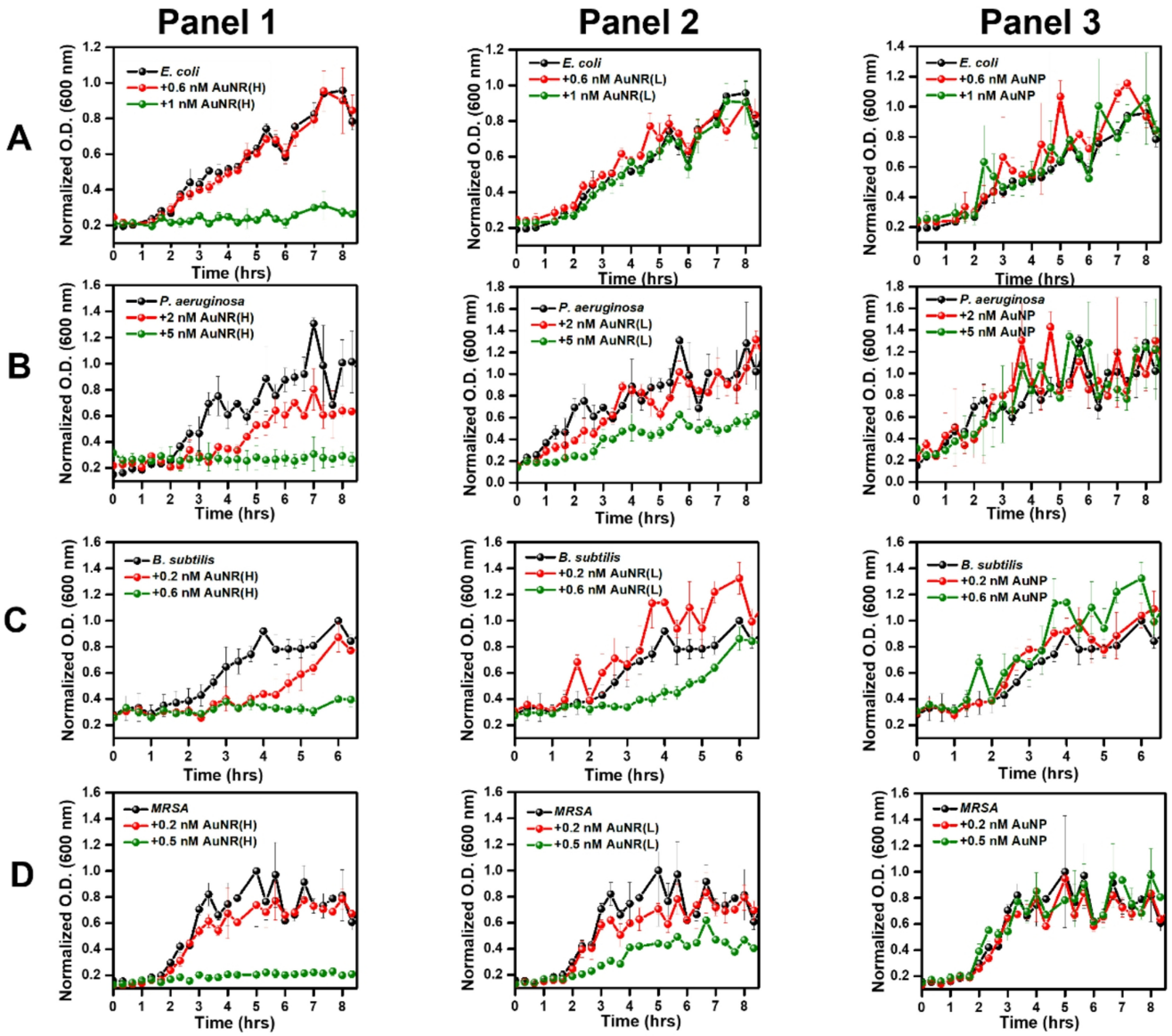


Fig. 2 Effect of different gold nanostructures: nanoparticles (AuNP), low aspect ratio nanorods (AuNR(L)), high aspect ratio nanorods (AuNR(H)) on the growth of **A***E. coli*, **B***P. aeruginosa*, **C***B. subtilis* and **D** MRSA

completely arrested the growth (Fig. 2C Panel 1). AuNR(L) at 0.2 nM concentration did not show significant change, while increasing the concentration to 0.6 nM increased the lag phase of *B. subtilis* growth as shown in Fig. 2C Panel 2. AuNPs at both concentrations did not inhibit *B. subtilis* growth, as shown in Fig. 2C Panel 3. Similar results were observed for MRSA, where growth was inhibited at 0.5 nM AuNR(H) concentration, and no effect on MRSA growth at 0.2 nM concentration of AuNR(H) was observed (Fig. 2D Panel 1). AuNR(L) at 0.2 nM was ineffective against MRSA growth, while the lag phase increased with 0.5 nM concentration (Fig. 2D Panel 2). No effect was observed on the growth of MRSA by AuNPs at either concentration (Fig. 2D Panel 3). The results mentioned above indicate that different bacterial species exhibited varying levels of susceptibility to the gold nanostructures at specific concentrations, highlighting the species-dependent response. Lower concentrations of AuNR (H) were sufficient to inhibit the growth of Gram-positive bacteria (*B. subtilis* and MRSA), while comparatively higher concentrations of AuNR(H) were required for Gram-negative (*E. coli* and *P. aeruginosa*). Also, at similar concentrations, AuNPs and AuNR(L) were not effective in inhibiting bacterial growth. Our findings demonstrate that AuNR(H) exhibits significantly greater anti-bacterial efficacy compared to AuNR(L) and AuNPs at equivalent concentrations. This variability underscores the importance of tailoring nanoparticle dosing to the target bacterial strain for optimal anti-bacterial performance. By systematically varying the concentrations, our results provided a comprehensive profile of gold nanostructures for effective growth inhibition across multiple species (Table 1).

Phototherapeutic effect of AuNR(H) on the growth of *E. coli* and *B. subtilis*

The phototherapeutic effect of AuNR(H) was evaluated by checking their photothermal and photodynamic properties. The photothermal effect is the ability of nanostructures to absorb light and convert it into localized heat, which can disrupt and kill bacterial cells. Whereas the production of reactive oxygen species (ROS) contributes to the photodynamic effect. We evaluated the photothermal efficacy of high-aspect-ratio gold nanorods (AuNR(H)) against *E. coli* and *B. subtilis* to determine their potential as photothermal agents for anti-bacterial applications. To assess this, bacterial cultures with AuNR(H) were irradiated with a near-infrared (NIR) laser (808 nm) at 1 W/cm² for 10 min. The AuNR(H) concentration was fixed at 0.6 nM for *E. coli* and 0.2 nM for *B. subtilis*. These concentrations were selected based on a previous set of experiments where AuNR(H) did not inhibit bacterial growth. In dark conditions, AuNR(H) did not exhibit bactericidal activity as expected. However, IR laser irradiation resulted in significant bacterial killing for both species, confirming the photothermal activation of AuNR(H), as shown in Fig. 3A and B.

It was known that spherical gold nanoparticles and nanorods can produce reactive oxygen species upon photoexcitation at their plasmonic wavelengths. We investigated ROS generation by AuNR(H) in the absence and presence of IR irradiation. *E. coli*, when incubated with AuNR(H) at 0.2 nM, showed a significant increase in ROS production even in the dark, and this effect was further pronounced in the presence of laser irradiation (Fig. 3C). Similar results were observed when *B. subtilis* was incubated with 0.2 nM of AuNR(H) under dark and light conditions (Fig. 3D). The enhanced ROS generation upon light exposure demonstrates that AuNR(H) effectively acts as a photosensitizer, enhancing oxidative stress in bacterial cells. ROS generation disrupts bacterial cell structures, offering a non-invasive and efficient method to target bacterial growth.

Effect of AuNR(H) on *E. coli* and *B. subtilis* biofilm formation

Further, we accessed the impact of AuNR(H) on biofilm formation by *E. coli* and *B. subtilis* using concentrations where bacterial growth remained unaffected (0.6 nM for *E. coli* and 0.2 nM for *B. subtilis*), ensuring that the observed effects were biofilm-specific and not growth-dependent. *E. coli* formed thick pellicle biofilms at the air-liquid interface, whereas biofilm formation was significantly reduced in the presence of AuNR(H), as observed through crystal violet staining images shown in Fig. 4A. The quantification of biomass indicated a $>90\%$ decrease in biomass compared

Table 1 Concentration-dependent growth Inhibition profile of gold nanostructures across multiple bacterial species

Bacterial species	Concentration of nanostructures (in nM)	Effect of Nanostructures		
		Nanorods AuNR (H) Inhibitory conc. (nM)	Nanorods AuNR (L)	Nanoparticles (AuNPs)
E. coli	0.6-1	1	No effect	No effect
P. aeruginosa	2–5	5	5 nM; increased lag phase	No effect
B. subtilis	0.2–0.6	0.6	0.6 nM; increased lag phase	No effect
Methicillin-resistant *S. aureus* (MRSA)	0.2-0.05	0.5	0.5 nM; increased lag phase	No effect

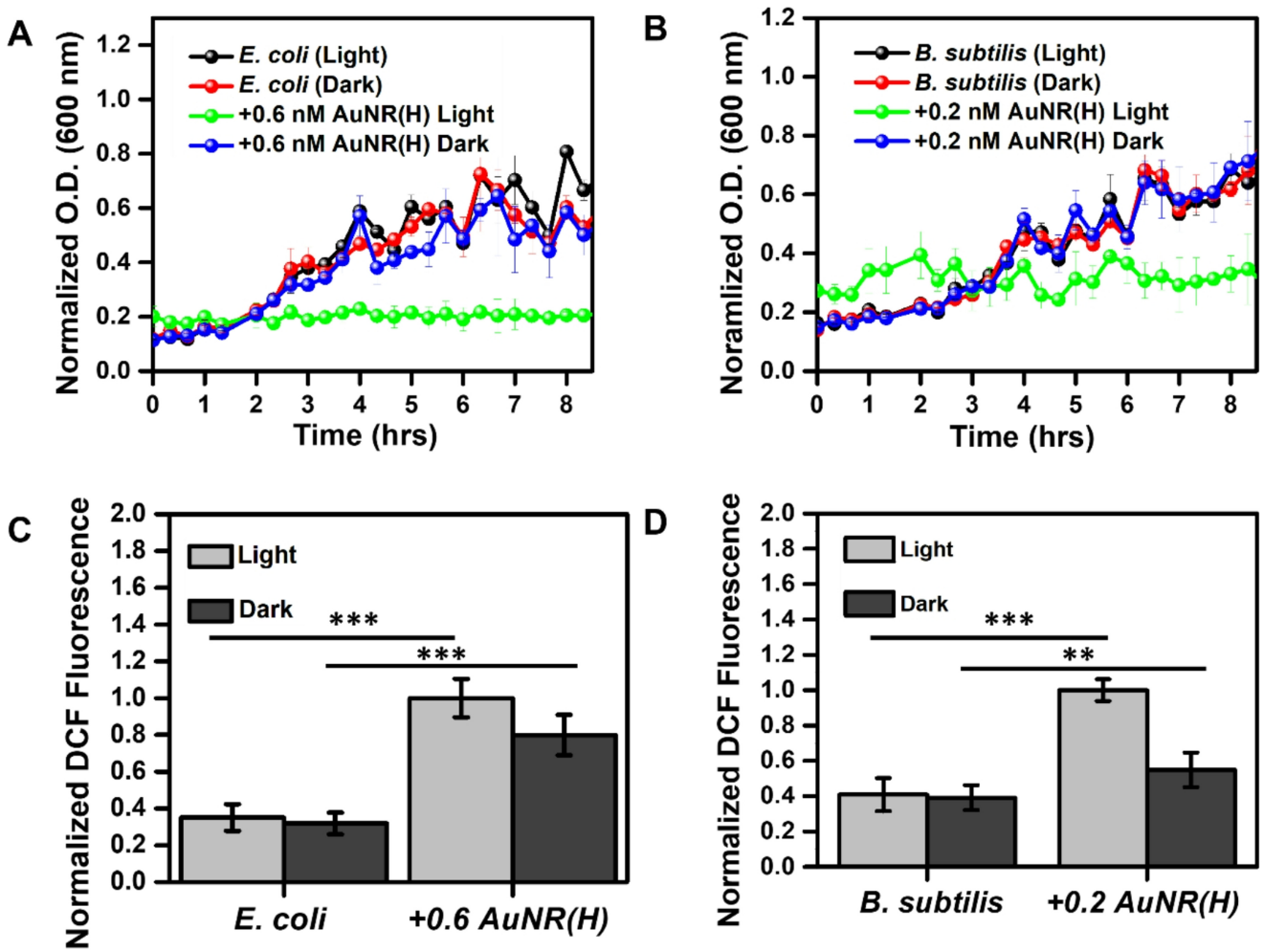


Fig. 3 Phototherapeutic (photothermal and ROS generation) effect of AuNR(H) on bacterial growth in the absence and presence of laser irradiation **A***E. coli*, **B***B. subtilis*, **C** ROS generation in *E. coli* and **D** ROS generation in *B. subtilis*

to the control (Fig. 4B). Further, the samples were observed under FE-SEM to observe the changes in extracellular polymeric matrix (EPM) and aggregation of the cells in the absence and presence of AuNR(H) under biofilm-forming conditions. We observed a dense network of cells in *E. coli* biofilm, whereas fewer scattered cells were observed when biofilms were treated with AuNR(H) (Fig. 4C). AuNR(H) exhibited similar properties in inhibiting *B. subtilis* biofilm at a concentration of 0.2 nM. No biofilms were observed in the presence of AuNR(H), whereas thick biofilm was observed in the absence of AuNR(H) (Fig. 4D). The quantification of *B. subtilis* biofilm biomass revealed a more than 90% decrease in the presence of AuNR(H), as depicted in Fig. 4E. Under FE-SEM, *B. subtilis* cells appeared to be clumped and covered with EPM in the absence of AuNR(H), but fewer clumps could be seen in the presence of 0.2 nM AuNR(H) (Fig. 4F).

These results demonstrate that AuNR(H) effectively inhibits biofilm formation independently of bacterial growth inhibition, highlighting its anti-biofilm activity. By focusing on concentrations that do not impact planktonic bacterial growth, this study underscores the specificity of AuNR(H) in targeting biofilm formation mechanisms, making it a promising approach for addressing biofilm-associated infections and reducing the challenge of antibiotic resistance.

Conclusions

Gold nanostructures, owing to their nanoscale size and tuneable surface properties, are highly versatile as their size, shape, and surface chemistry can be engineered to optimize antimicrobial activity and reduce toxicity to host cells (Mutalik et al. 2023; Kumalasari et al. 2024). Our study demonstrates the anti-bacterial and anti-biofilm efficacy of high-aspect-ratio gold nanorods (AuNR(H) compared to low-aspect-ratio nanorods (AuNR(L) and spherical nanoparticles (AuNPs) across a range of clinically and

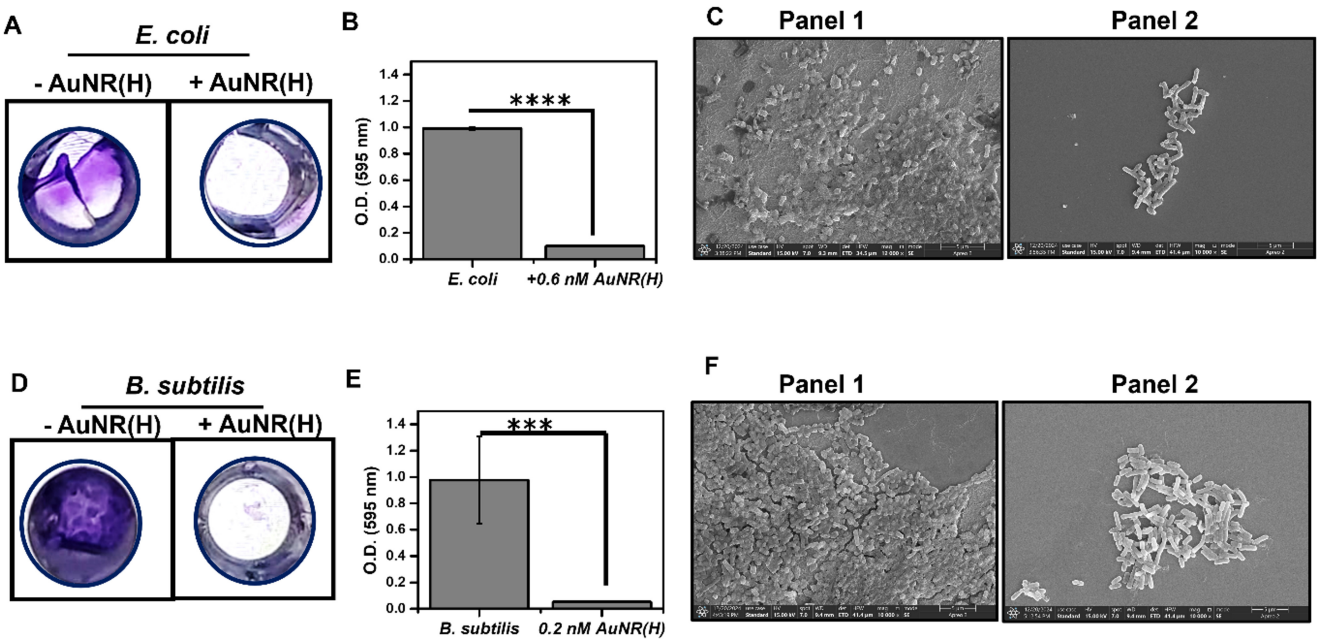


Fig. 4 Effect of AuNR(H) on biofilm growth; **A** Crystal violet-stained images of *E. coli* biofilms, **B***E. coli* Biofilm biomass quantification, **C** FESEM images of *E. coli* biofilms in the absence (panel 1) and presence (panel 2) of 0.6 nM AuNR(H). **D** Crystal violet-stained images of *B. subtilis* biofilms, **E***B. subtilis* biofilm biomass quantification, and **F** FESEM images of *B. subtilis* biofilms in the absence (panel 1) and presence (panel 2) of 0.2 nM AuNR(H)

environmentally relevant bacterial species. The distinct advantages of AuNR(H) at lower concentrations include their ability to inhibit bacterial growth, induce reactive oxygen species (ROS) generation under light irradiation, and prevent biofilm formation independently of bacterial growth effects. The photothermal and photodynamic activation of AuNR(H) further highlights their versatility as a dual-action anti-bacterial agent. Our findings suggest that the high aspect ratio of nanorods is more effective at lesser concentrations as compared to low aspect ratio nanorods and nanoparticles and offers a promising solution for combating antibiotic-resistant infections and biofilm-associated complications. By optimizing nanoparticle size, shape, and spatial distribution, a new frontier emerges in combating bacterial and biofilm-associated infections and advancing the field of antimicrobial nanotechnology.

Supplementary Information The online version contains supplementary material available at https://doi.org/10.1007/s43538-025-00490-3.

Acknowledgements The authors acknowledge the Centre for Research and Development of Scientific Instruments (CRDSI) Facility at the Indian Institute of Technology Jodhpur for access to the FE-SEM. NJ acknowledges seed grant (I/Seed/NJ/20190019) from the Indian Institute of Technology Jodhpur. RV acknowledges funding support by the Department of Biotechnology (DBT), Government of India, for the Ramalingaswami Biomedical Fellowship (BT/RLF/Re-entry/17/2018), seed Grant (I/SEED/RRV/20200076) funded by Indian Institute of Technology Jodhpur, and Core Research Grant funded by SERB (CRG/2023/001189). Research fellowship through CSIR to HA and through MoE to RKS is duly acknowledged.

References

Agarwal, H., Gurnani, B., Pippal, B., et al.: Capturing the micro-communities: insights into biogenesis and architecture of bacterial biofilms. BBA Adv. **7**, 100133 (2025)

Azeem, K., Fatima, S., Ali, A., et al.: Biochemistry of bacterial biofilm: insights into antibiotic resistance mechanisms and therapeutic intervention. Life. **15**, 49 (2025)

Johnson, C.J., Dujardin, E., Davis, S.A., et al.: Growth and form of gold nanorods prepared by seed-mediated, surfactant-directed synthesis. J. Mater. Chem. **12**, 1765–1770 (2002)

Kumalasari, M.R., Alfanaar, R., Andreani, A.S.: Gold nanoparticles (AuNPs): a versatile material for biosensor application. Talanta Open **9**, 100327 (2024)

Liu, X., Atwater, M., Wang, J., et al.: Extinction coefficient of gold nanoparticles with different sizes and different capping ligands. Colloids Surf. B Biointerfaces **58**, 3–7 (2007)

Liu, H.Y., Prentice, E.L., Webber, M.A.: Mechanisms of antimicrobial resistance in biofilms. npj Antimicrob. Resist. **2**, 1–10 (2024)

Mishra, A., Aggarwal, A., Khan, F.: Medical device-associated infections caused by biofilm-forming microbial pathogens and controlling strategies. Antibiot (Basel) **13**, 623 (2024)

Murphy, C.J., Sau, T.K., Gole, A.M., et al.: Anisotropic metal nanoparticles: synthesis, assembly, and optical applications. J. Phys. Chem. B. **109**, 13857–13870 (2005)

Mutalik, C., Saukani, M., Khafid, M., et al.: Gold-based nanostructures for antibacterial application. Int. J. Mol. Sci. **24**, 10006 (2023)

Rolfe, M.D., Rice, C.J., Lucchini, S., et al.: Lag phase is a distinct growth phase that prepares bacteria for exponential growth and involves transient metal accumulation. J. Bacteriol. **194**, 686–701 (2012)

Saed, M., Ayivi, R.D., Wei, J., et al.: Gold nanoparticles antibacterial activity: Does the surface matter? Colloid Interfac Sci. **62**, 100804 (2024)

Sahoo, K., Meshram, S.: Biofilm formation in chronic infections: a comprehensive review of pathogenesis, clinical implications, and novel therapeutic approaches. Cureus **16**:e70629 (2024)

Publisher's note Springer Nature remains neutral with regard to jurisdictional claims in published maps and institutional affiliations.

Springer Nature or its licensor (e.g. a society or other partner) holds exclusive rights to this article under a publishing agreement with the author(s) or other rightsholder(s); author self-archiving of the accepted manuscript version of this article is solely governed by the terms of such publishing agreement and applicable law.